Receptivity characteristics of under-expanded supersonic impinging jets

Shahram Karami [1]†, Paul C. Stegeman [1], Andrew Ooi [2], Vassilis Theofilis [3,4] AND Julio Soria [1,5]

[1] Laboratory for Turbulence Research in Aerospace & Combustion (LTRAC), Department of Mechanical and Aerospace Engineering, Monash University, Melbourne 3800, Australia

[2] Department of Mechanical Engineering, University of Melbourne, Victoria 3010, Australia

[3] School of Engineering, University of Liverpool, Liverpool, L69 7ZX, UK

[4] Department of Mechanical Engineering, University of São Paulo, Av. Prof. Mello Moraes, 2231, São Paulo, Brazil

[5] Department of Aeronautical Engineering, King Abdulaziz University, Jeddah 21589, Kingdom of Saudi Arabia

(Received ?; revised ?; accepted ?. - To be entered by editorial office)

The receptivity of an under-expanded supersonic impinging jet flow at the sharp nozzle lip to acoustic impulse disturbances is investigated as a function of geometric and flow parameters. The under-expanded supersonic jets emanate from an infinite-lipped nozzle, *i.e.* the nozzle exit is a circular hole in a flat plate. Two specific cases have been investigated correspond to nozzle-to-wall distances of $h = 2d$ and $5d$, where d is the jet diameter, at a nozzle pressure ratio $NPR = 3.4$ and a Reynolds number of 50,000.

Receptivity in this study is defined as originally coined up by Morkovin (1969) (see also Reshotko (1984)) as the internalisation of an external disturbance into the initial condition that either initiates or sustains a vortical fluid dynamic instability. Notionally, receptivity can be considered as a transfer function between the external disturbance and the initial conditions of the vortical instability. In the case of under-expanded supersonic impinging jet flow subjected to an acoustic disturbance this transfer function is located at the nozzle lip and thus, is amenable to an impulse response analysis using the linearised compressible three-dimensional Navier-Stokes equations. In this study, the transfer function at the nozzle lip is defined as the ratio of the output flow energy to the input acoustic energy of the acoustic disturbance. The sensitivity of this transfer function to the angular acoustic disturbance location, its azimuthal mode-number and Strouhal number has been investigated for the two under-expanded supersonic impinging jet flow cases.

It is found that for both the $h = 2d$ and $5d$ cases, acoustic disturbances located at angles greater than 80° from the jet centreline, with Strouhal numbers in the range between 0.7 and 6.5 have the highest receptivity for all azimuthal mode-numbers investigated, except the azimuthal mode-number 2 in the case of $h = 5d$. The case with $h = 5d$ is found to also have high receptivity to acoustic disturbances located at angles between 15° and 50° from the jet centreline for acoustic disturbances of all azimuthal mode-numbers.

Key words:

† Email address for correspondence: shahram.karami@monash.edu

1. Introduction

Under-expanded supersonic jets form when the static pressure at the choked nozzle exit is higher than the ambient pressure. Their applications in engineering ranges from exhausts of aircraft and rockets to mixing processes in supersonic combustors, accidental leakage of pressurised fluids and advanced cold spray additive manufacturing processes such as the cold-spray process (Li *et al.* 2012). Under-expanded jets have been the subject of intense research since they were first described theoretically by Prandtl and his Göttingen group (Prandtl 1904, 1907, 1913; Ackeret 1927). The acoustic-flow instability associated with the under-expanded supersonic impinging jet is known to cause self-sustained oscillations (Henderson 1966; Donaldson *et al.* 1971). The high level of oscillations on the impinged surface can damage the surface structure and lead to material fatigue, while in advanced cold spray manufacturing, high-amplitude pressure oscillations affect affects the quality of the deposited coating. Such oscillations have been observed in other configurations, for instance, subsonic impinging jets (Ho & Nosseir 1981; Tam & Ahuja 1990), a resonance tube, an edge-tone and a plate with a cavity (Raman & Srinivasan 2009). Many of the aspects associated with the self-sustained nature of the oscillations in these flows have been analysed and predicted in the context of linear dynamics (Hammond & Redekopp 1997; Haddad & Corke 1998; Erturk & Corke 2001; Wanderley & Corke 2001; Pier 2002; Barkley 2006; Sipp & Lebedev 2007; Mittal 2008; Oberleithner *et al.* 2014; Turton *et al.* 2015; Sartor *et al.* 2015; Beneddine *et al.* 2016; Ruban *et al.* 2016; Illingworth *et al.* 2018). A linear dynamics approach is also the approach that we have utilised in the present study.

The accepted conceptual theory describing the feedback oscillations in supersonic impinging jets is due to Powell (1988), which is an analogue of the Rossiter mechanism found in open cavity flow (Rossiter 1964). The feedback loop is based on the interactions between the aero-acoustic field, which in under-expanded supersonic jet flows has a number of sources as depicted in figure 1 and the jet flow as evidenced in the ultra-high-speed flow visualisation of Risborg & Soria (2009) and Soria & Risborg (2019). As can be clearly evidenced in these ultra-high-speed schlieren visualisations, shear-layer disturbances develop in the form of Kelvin-Helmholtz (K-H) instabilities as shown diagrammatically by the blue arrow in the shear layer of the jet depicted in figure 1, which subsequently interact with the oblique shock, Mach disk and stand-off shock. These interactions displace the shocks, creating high-intensity acoustic waves at the shock locations and impinging region, as shown in figure 1, which travel upstream towards the jet orifice via the quiescent flow domain outside of the supersonic jet. As the circumferential edge of the jet expands upon exit from the nozzle in an under-expanded supersonic jet, some or all of these acoustic waves are blocked from directly reaching the jet nozzle lip. However, the acoustic waves are also reflected by the surrounding structures and the reflected waves can reach the nozzle lip and can be internalised into the initial conditions for a shear-layer instability at the nozzle lip via a receptivity mechanism and hence, close the feedback loop. Clear visualisation of this process can be observed in figure 11 of Risborg & Soria (2009) and the corresponding ultra-high-speed movie in Soria & Risborg (2019).

Considerable evidence for the feedback loop being the mechanism responsible for the self-sustained oscillations has been accumulated via many experimental studies of supersonic impinging jets (Henderson & Powell 1993; Henderson *et al.* 2005; Risborg & Soria 2009; Mason-Smith *et al.* 2015; Soria & Risborg 2019). However, our understanding of the feedback loop ingredients is not complete, particularly from a quantitative point of view. The forward and backward paths of the feedback loop are a flow instability in the shear layer of the jet and an acoustic wave propagating in the medium, respectively. The

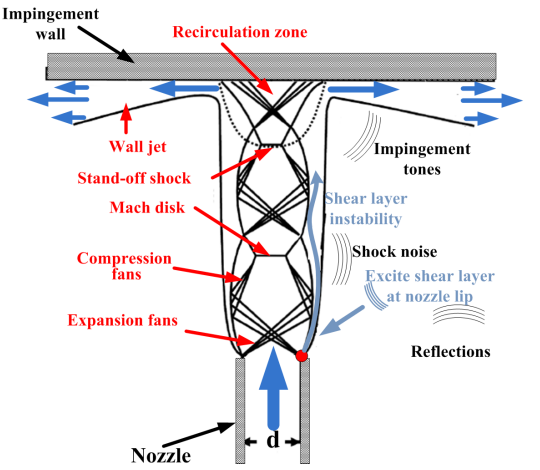

FIGURE 1. Schematic of an under-expanded supersonic impinging jet.

flow instabilities subsequently develop into large-scale coherent vortical structures in the shear layer of the jet. The downstream convection of these structures has been observed in many experimental and numerical studies of free and impinging under-expanded supersonic jets (Powell 1988; Edgington-Mitchell *et al.* 2014*b*; Mason-Smith *et al.* 2015; Gojon *et al.* 2015; Stegeman *et al.* 2015; Amili *et al.* 2016; Gojon & Bogey 2017). A prevailing belief is that the acoustic waves scattered by the nozzle lip are the source that drive the convective K-H instability, which subsequently develop into these coherent structures (Henderson *et al.* 2005; Powell 1988). However to-date, the mechanism that converts irrotational acoustic waves into the initial condition for the convective K-H instabilities at the jet nozzle in terms of the flow geometry and parameters of the supersonic under-expanded impinging jets has not been quantitatively analysed. This mechanism is clearly one which falls within the realms of the term *receptivity* as coined up by Morkovin (1969) and Reshotko (1984) and defined as the internalisation of an external disturbance into the initial condition that either initiates or sustains a vortical fluid dynamic instability. In the context of this study, this process can be most visually observed in figure 11 of Risborg & Soria (2009) and the corresponding ultra-high-speed movie in Soria & Risborg (2019), which clearly shows the initial condition of a K-H instability in the shear layer when the acoustic wave hits the jet lip closest for an inclined plate in an under-expanded supersonic jet impinging on an inclined plate.

Receptivity in a number of flows has been studied since the early 1970s with a heavy concentration on boundary layer receptivity (Jones & Morgan 1972, 1973; Morgan 1974; Bechert 1988; Bechert & Stahl 1988; Kerschen 1996; Wanderley & Corke 2001; Haddad & Corke 1998; Erturk & Corke 2001; Ruban *et al.* 2016). In addition, most of the other studies have been associated with the trailing edge flow from a splitter plate where a simple vortex-sheet model with an infinite extent splitter plate was considered. Kerschen (1996) studied the sensitivity of shear-layer instability waves formed at the trailing edge of a splitter plate to acoustic source location using a vortex-sheet model. Acoustic sources near and far from the trailing edge on both sides of the splitter plate were considered. The flow on one side of the splitter plate was quiescent, while it was either supersonic or subsonic on the other side of the plate. This study found that the development of shear-layer instability waves are more sensitive to the excitation on the flow side of the splitter plate compared to the excitation on the quiescent side of the plate. It was also

observed that the receptivity to these acoustic disturbances decreases as the acoustic source location is moved away from the trailing edge. The influences of the sharpness of the leading edge and angle of acoustic incident were studied by Haddad & Corke (1998) and Erturk & Corke (2001) using the linearised Navier-Stokes equations. This study found that the leading-edge receptivity increases with the sharpness of the leading edge.

Tam (1986) proposed that for a two-dimensional shear layer developing from a splitter plate a necessary condition for the reception of acoustic waves by the lip of the splitter plate and hence, the formation of K-H instabilities, was that the spatial wavenumber and temporal frequency of the shear layer instability and the acoustic wave must match. Barone & Lele (2005) utilised the linearised Navier–Stokes equations with small-amplitude mass, momentum, and heat sources in the vicinity of a mixing layer to study the receptivity of a compressible mixing layer. This study showed that not only does the receptivity depend on the frequency and the location of the excitation source but it also depends on the source type. The primary focus of these prior studies of receptivity has been confined to the relatively simple configuration of the mixing layer subjected to forcing via an external source, with only a few studies related to self-sustained flows (Rowley *et al.* 2002). In the study by (Rowley *et al.* 2002), the frequency dependence of the receptivity, which occurs at the upstream edge of the cavity of the self-sustained flow over a rectangular cavity, was ignored. This assumption is as stated by (Rowley 2002) was considered "a crude model".

As pointed out numerous experimental and numerical studies of supersonic impinging jets have been conducted, the focus of theses studies were on the large coherent structures with little attention paid to the initial mechanism that leads to the generation of the instability that subsequently evolves into these large scale coherent vortical structures. To the best of our knowledge, the receptivity of under-expanded supersonic free or impinging jets has not previously been investigated. Hence, the primary objective of this paper is to address this gap by analysing the receptivity in under-expanded supersonic impinging jets. To achieve this goal, this paper seeks to quantify the transfer function of the *receptivity* and its dependency on location, frequency and azimuthal mode-number of the acoustic source.

The manuscript is organised as follows. In section 2, the framework of the receptivity analysis within the structure of the linearised Navier-Sokes equations is presented. The mean flow required for the linearised Navier-Stokes equations is the mean flow obtained from large-eddy simulations (LES) of under-expanded supersonic impinging jets and is presented in section 3. The results including the mean flow fields and a comprehensive discussion of the receptivity, which is the primary focus of this study, and interpretation of the results are presented in section 4. Concluding remarks are presented in section 5.

2. Framework of the receptivity analysis

The aim of the receptivity analysis is to quantify the system response to external forcing. As stated above, receptivity in this case is defined as the internalisation of the acoustic waves into the initial condition of the shear-layer instabilities at the sharp edge of the nozzle lip. Therefore, there is a need to quantify the acoustic irrotational field and vortical fluid flow field in the limit as the sharp edge of the nozzle lip is approached, *i.e.* as the points $s = 0$ in figure 2 is approached from s_{in} and s_{out} respectively. The receptivity in this context is characterised by a transfer function at the nozzle lip, which is defined as the ratio of the output energy of the rotational flow to the input acoustic irrotational energy in the limit where the locations of both these energies approach the point $s = 0$, *i.e.* the nozzle lip. Therefore, the lip of the nozzle can be considered a linear transformer,

because receptivity is considered to be linear (Haddad & Corke 1998; Erturk & Corke 2001). This permits us to employ the linearised Navier-Stokes equations to quantitatively study the receptivity in under-expanded supersonic impinging jet flows.

Modal linear stability theory has been used widely in the past to reveal the underpinning physics of unsteady flows (Hammond & Redekopp 1997; Pier 2002; Barkley 2006; Sipp & Lebedev 2007; Mittal 2008; Oberleithner *et al.* 2014; Turton *et al.* 2015; Sartor *et al.* 2015; Beneddine *et al.* 2016; Illingworth *et al.* 2018). Receptivity, however, as pointed out by Reshotko (1976), is different from instability both physically and mathematically. It is a transformation of acoustic irrotational disturbances into vortical fluid dynamic instabilities. The problem is not homogeneous and a normal mode analysis (*i.e.* eigenvalue problem) cannot be used. Instead the solution of the linearised Navier-Stokes equations with external forcing is required (Reshotko 1976). This assumption is consistent with that used in the previous studies of the leading-edge receptivity (Haddad & Corke 1998; Erturk & Corke 2001) where the receptivity is considered to be a linear process for weak disturbances that permits the application of the linearised Navier-Stokes equations in the analysis.

The linearised compressible Navier-Stokes equations (LNSE) are derived by superimposing small-amplitude disturbances on a mean flow. Denoting the mean flow variables as $\overline{(...)}$ and perturbations as $(...)'$, the linearised compressible Navier-Stokes equations are given as

$$\begin{aligned}
\frac{\partial \rho'}{\partial t} &= -\nabla \cdot (\rho \mathbf{u})', \\
\frac{\partial (\rho \mathbf{u})'}{\partial t} &= -\nabla \cdot (\overline{\rho}\overline{\mathbf{u}} \otimes \mathbf{u}' + (\rho \mathbf{u})' \otimes \overline{\mathbf{u}}) - \nabla p' + \overline{\mu} \nabla \cdot \mathbb{T}', \\
\frac{\partial (\rho e)'}{\partial t} &= -\nabla \cdot \left(\overline{(\rho e + p)} \mathbf{u}' + (\rho e + p)' \overline{\mathbf{u}} \right) + \overline{k} \nabla^2 T' + \overline{\mu} V_{KE},
\end{aligned} \tag{2.1}$$

where

$$\begin{aligned}
V_{KE} &= \left((\nabla \cdot \mathbb{T}') \cdot \overline{\mathbf{u}} + (\nabla \cdot \mathbb{T}') \cdot \mathbf{u}' + \mathbb{T}' : \nabla \overline{\mathbf{u}} + \overline{\mathbb{T}} : \nabla \mathbf{u}' \right), \\
\mathbb{T} &= \nabla \mathbf{u} + (\nabla \mathbf{u})^T - \frac{2}{3} (\nabla \cdot \mathbf{u}) \mathbb{I},
\end{aligned} \tag{2.2}$$

and the linearised version of the equation of state is

$$p' = \frac{\overline{\rho} T' + \rho' \overline{T}}{\gamma}. \tag{2.3}$$

Finally, the viscosity and thermal conductivity are given by

$$\overline{\mu} = \frac{\overline{T}^{0.76}}{\mathrm{Re}} \qquad \text{and} \qquad \overline{k} = \frac{\overline{\mu}}{\gamma - 1} \frac{1}{\mathrm{Pr}}. \tag{2.4}$$

These equations are commonly presented in the concise matrix form

$$\frac{\partial q'}{\partial t} = \mathbb{A} q', \tag{2.5}$$

where q' represents the perturbations $(\rho', u_x', u_r', u_\theta', e')$, and $\mathbb{A}$ is the linear operator advancing the small perturbations in time.

The above equations are non-dimensionalised as follows with the superscript '*' rep-

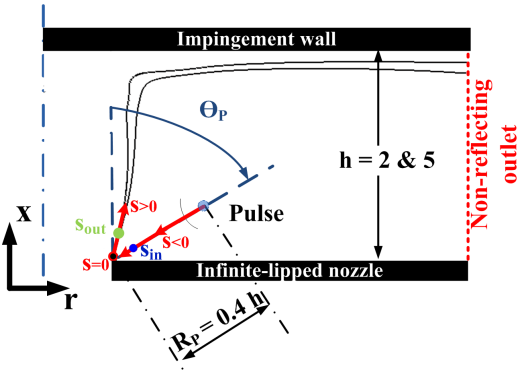

FIGURE 2. Schematic of the impinging jet with relevant parameters of the receptivity analysis (Impulse is located with in a radius of $R_p = 0.4h$ from the nozzle and angle of θ_p from the jet axis. The black solid line represents the sonic-line in a typical under-expanded supersonic jet.).

resenting dimensional values, while the subscript 'o' refers to ambient conditions:

$$x_j = \frac{x_j^*}{d}, \quad U_j = \frac{U_j^*}{a_o^*}, \quad \rho = \frac{\rho^*}{\rho_o^*}, \quad t = \frac{t^* a_o^*}{d}, \quad p = \frac{p^*}{\rho_o^* a_o^{*2}},$$
$$T = \frac{T^*}{\gamma T_o^*}, \quad \mu = \frac{\mu^*}{\mathrm{Re}\mu_o^*}, \quad \mathrm{Pr} = \frac{\upsilon^*}{\alpha^*}, \quad \mathrm{Re} = \frac{\rho_o^* a_o^* d}{\mu_o^*} \quad St = fd/a_o^*. \tag{2.6}$$

In these equations, x_j represents the spatial vector, d the jet diameter, U_j the velocity vector, a the speed of sound, ρ the density, T the temperature, t time (acoustic time unit †), p the pressure, γ the heat capacity ratio, f the frequency, St the Strouhal number, and μ the dynamic viscosity, which is given by $\mu/\mu_o = (T/T_o)^{0.7}$. The variable Re represents the Reynolds number and Pr the Prandtl number.

The configuration of the under-expanded impinging jet is characterised by a nozzle–to–wall distance denoted by h. The jets emanate from an infinite-lipped nozzle (*i.e.* a circular hole in a flat plate) which is referred to as the nozzle lip throughout the rest of the manuscript. An acoustic impulse described by,

$$p'(t=0) = A\, exp\left(-\frac{(x-x_o)^2}{2\sigma_x^2} - \frac{(r-r_o)^2}{2\sigma_r^2}\right)\cos(2\pi m\theta), \tag{2.7}$$

is used as a localised initial condition of the acoustic irrotational pressure fluctuations, where 'A' is the amplitude of the impulse; x_o and r_o are the streamwise and radial location of the centre of the impulse, respectively; σ_x and σ_r are the radii of the impulse in the streamwise and radial directions, respectively with σ_x and $\sigma_r << \lambda$ the acoustic wavelength and m is the azimuthal mode-number. To study the sensitivity of amplification of the incoming wave at the nozzle lip to the impulse location, the centre of the impulse is located at a radius of $R_p = 0.4h$ from the nozzle lip and an angle of θ_p where θ_p is the angle from the jet axis as shown in figure 2. This corresponds to the location of the impulse in the axial and the radial directions of $x_o = R_p \sin(\theta_p)$ and $r_o = R_p \cos(\theta_p)$. Full details of the under-expanded supersonic impinging jet configuration are presented in figure 2. $R_p = 0.4h$ is chosen to maintain an adequate resolution of the propagating wave as a stretched grid is used in the radial direction (see figure 6) and to obtain well-separated input and output signals with no overlap for the purpose of the receptivity analysis.

† Note that the acoustic time unit in the configuration of this study is equivalent to the characteristic time of a jet flow based on the inlet velocity and jet diameter as the nozzle is chocked in under-expanded supersonic jets, hence the inlet Mach number is unity.

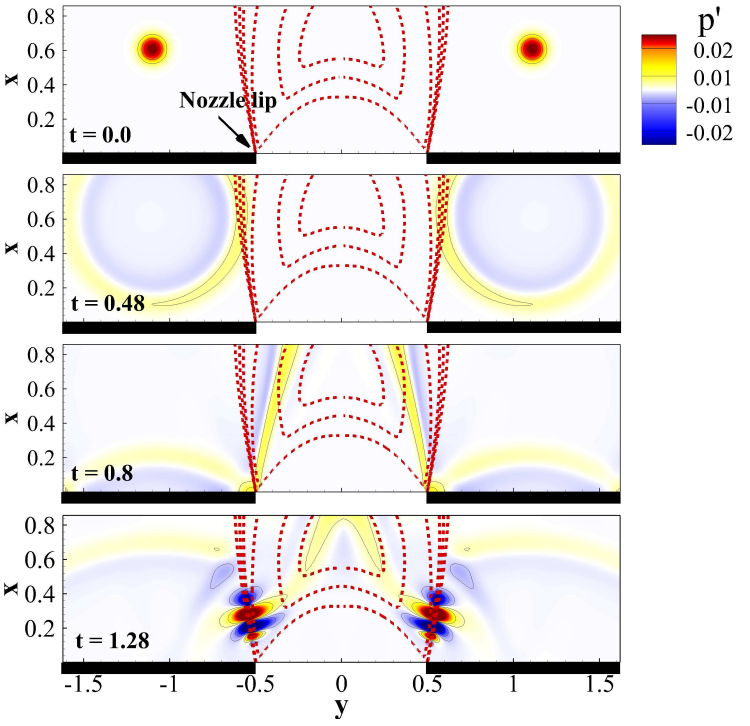

FIGURE 3. Instantaneous contours of the pressure fluctuation field of the pressure impulse simulation for the nozzle-to-wall distance of 2 jet diameters where impulse is located at $R_p = 0.8$ and $\theta_p = 45^\circ$ (y is related to radius by $-r < y < r$).

Using a mean flow field, the linearised Navier-Stokes equations can be solved to obtain the time evolution of the flow disturbances to the impulse. The time evolution of perturbations for the case where the impulse is located at $\theta_p = 45^\circ$ is presented in figure 3. The initial condition (t=0) is started by a pressure impulse. The pressure wave formed by the impulse travels in the medium and reaches the nozzle lip at t=0.8. It is internalised into a shear-layer instability and forms a convective instability as shown in figure 3 at t=1.28.

To obtain a better understanding of the receptivity process, the transfer function between the input and output energy of the disturbance at the nozzle lip is required. The input is located on the straight line connecting the source to the nozzle lip (blue dot marked on s_{in} in figure 2) and the output is located in the shear layer of the jet as close as possible to the nozzle lip (green dot marked on s_{out} in figure 2). A new one-dimensional coordinate is defined as s. It is centred at nozzle lip marked by $s = 0$ in figure 2. Any location on the straight line from the nozzle lip to the impulse acoustic source has a negative sign increasing towards the source location ($s < 0$) and any location at the shear layer has a positive sign in this coordinate which is increasing by moving away from the nozzle lip ($s > 0$). The fluctuation of the density-weighted kinetic energy of the disturbance is defined as

$$E = \frac{1}{2}\left[2\overline{\rho u_i}u_i' + \overline{\rho}u_i'^2 + \rho'\overline{u_i}^2 + 2\rho' u_i'\overline{u_i} + \rho' u_i'^2\right]. \tag{2.8}$$

The time history of E on the s coordinate for the linearised simulation for a case with a pressure impulse at $R_p = 0.8$ and $\theta_p = 45^\circ$ is presented in figure 4a. The white solid

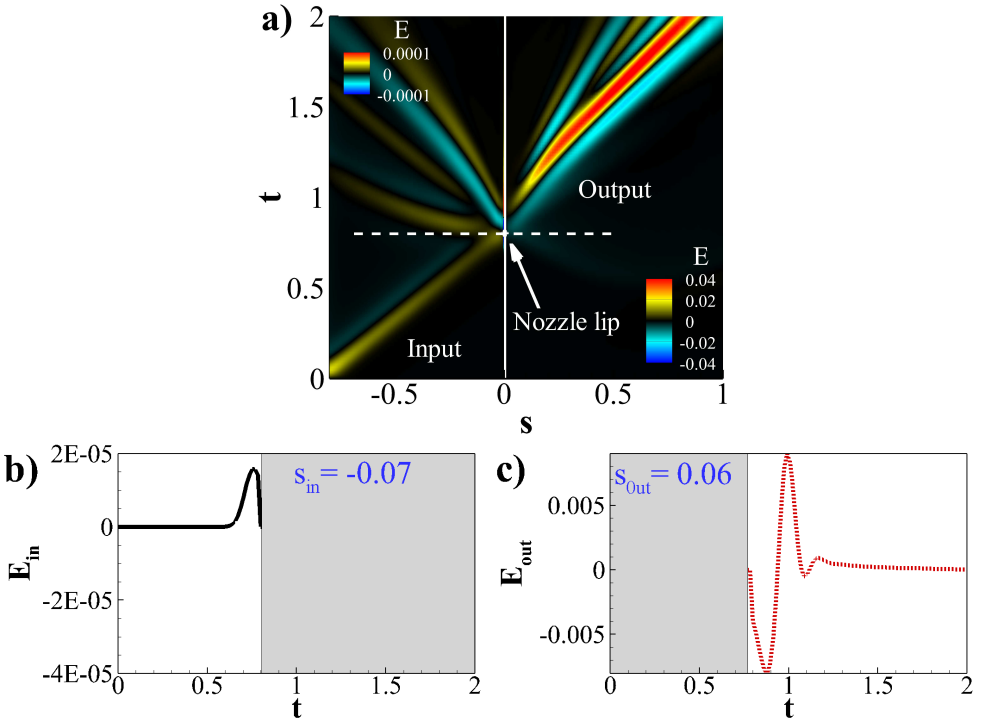

FIGURE 4. a) the signal history on new coordinate s (the colourmaps of input signal (s <0) and output signal (s >0) are adjusted as shown on top-left and bottom-right sides, respectively) b) input and c) output signals with relevant time cut-off for the case with the nozzle-to-wall distance of 2 jet diameters for the same case as in figure 3.

line provides the location of the nozzle lip, $s = 0$, and the white dashed line shows the instance when the pressure wave, generated by the acoustic impulse reaches the nozzle lip. Note that the colorbars of the left and right sides of the solid white line have different scales and adjusted for demonstration purposes, the acoustic energy is much smaller than the resulting fluid dynamic energy. The input signal must be sampled in the bottom left quarter of this plot, while the output signal must be sampled in the top right quarter of this plot. To obtain a representative form of the transfer function of the receptivity as per the definition, the acoustic energy and hydrodynamic energy must be evaluated as $s_{in} \to 0$ and $s_{out} \to 0$, respectively. However, the minimum values of s_{in} and s_{out} are limited by the ability to distinguish the input and output signals at the sample points which in turn is limited by the spatial resolution of the numerical grid. Therefore, the values of $s_{in} = -0.07$ and $s_{out} = 0.06$† are selected in this analysis. Typical input and output signals at s_{in} and s_{out} are presented in figures 4 (b) and (c). Assuming a linear time-invariant relationship between the input and the output, the output can be predicted by a convolution along time between the input variable and a convolution kernel (Sasaki *et al.* 2019) given by

$$E_{out}(t) = \int_{-\infty}^{\infty} g(\tau) E_{in}(t-\tau) d\tau, \tag{2.9}$$

† Note that these values are non-dimensionalised with respect to the jet diameter.

TABLE 1. Numerical and physical parameters of the receptivity analysis

Radius of the impulse location (R_p)	$0.4h$
Angular position of the impulse (θ_p)	10° - 85° with an incrementation of 5°
The radii of the impulse in the streamwise (σ_x)	0.05
The radii of the impulse in the radial direction (σ_r)	0.05
Amplitude of the impulse (A)	$0.01\bar{P}_{(x_o,r_o)}$
Input location on the s coordinate (s_{in})	-0.07
Output location on the s coordinate (s_{out})	0.06
Azimuthal mode-number (m)	$0, 1, 2$

where $g(\tau)$ is the convolution kernel which also referred to as time-invariant transfer function. In order to obtain this convolution kernel, it is more convenient to formulate the problem in the frequency space. In the frequency domain, the frequency response can be obtained from the auto-spectrum of the input and cross-spectra between the input and output signals (Bendat & Piersol 2011; Sasaki *et al.* 2019). Hence, the transfer function in the frequency domain is defined as

$$G(St) = \frac{||\hat{E}_{out}(St)\hat{E}^*_{in}(St)||}{||\hat{E}_{in}(St)\hat{E}^*_{in}(St)||}, \tag{2.10}$$

where St is the Strouhal number, $\hat{E}$ is the Fourier transform of the fluctuations of the density-weighted kinetic energy of the flow.

In order to study the effect of the acoustic impulse location on the receptivity, the angular position of the acoustic impulse is varied from a position close to the impingement wall ($\theta_p = 10^\circ$) to one near the infinite-lipped nozzle wall ($\theta_p = 85^\circ$) using angular increments of 5°. This study is limited to the first three azimuthal mode-numbers as they are found to be the dominant modes based on previous studies (Weightman *et al.* 2017). Full details of all the parameters and their values for the receptivity analysis are presented in table 1.

3. Large-eddy simulation - determination of the mean flow

An in-house parallel high-fidelity LES code with a novel shock identification and capturing method was used to undertake the necessary LES to determine the mean flow associated with the under-expanded supersonic impinging jet. The code, which has been tested and validated in previous studies (Stegeman *et al.* 2016*a*,*b*; Karami *et al.* 2018*a*,*b*; Karami & Soria 2018; Karami *et al.* 2019), solves the filtered compressible conservation equations of mass, momentum, and total energy in cylindrical coordinates. The subgrid-scale terms are computed using the Germano's dynamic model with the adjustment proposed by Lilly (1992). A sixth-order central finite difference method is used for spatial discretisation in the smooth regions, while a fifth-order weighted essentially non-oscillating scheme (WENO) with local Lax-Friedrichs flux splitting is used in the discontinuous regions. The temporal integration is performed using a fourth-order five-step Runge-Kutta scheme (Kennedy & Carpenter 1994; Kennedy *et al.* 2000). The locally one-dimensional inviscid compressible boundary condition proposed by Poinsot & Lele (1992) is employed at the far-field outflow boundaries. For further details on the numer-

Table 2. Computational grid of LES

Nozzle-to-wall distance (h/d)	$N_x \times N_r \times N_\theta$
2	$480 \times 432 \times 96$
5	$608 \times 632 \times 96$

ical method, the novel shock identification and capturing method and LES code, the interested reader is referred to Karami *et al.* (2019).

The ratio between the stagnation pressure measured in the jet plenum and the ambient pressure, commonly referred as nozzle pressure ratio $NPR = 3.4$ for all cases considered. This NPR is higher than the critical NPR (*i.e.* here for dry air critical NPR = 1.893), hence, the nozzle is chocked and the nozzle exit Mach number is unity. Parameters addressed in the present work are guided by the recent experimental studies of under-expanded supersonic impinging jets of Mason-Smith *et al.* (2015) and Amili *et al.* (2016), who found that the nozzle pressure ratio of 3.4 leads to the initial formation of a small Mach disk. They also observed that an increase in the nozzle pressure ratio enlarges the size of the Mach disk. Hence, a nozzle pressure ratio of 3.4 was selected for this numerical study, as being the case where the Mach disk forms from the converging point between the expansion and compression waves.

Experimental and numerical studies of the same configuration (Ho & Nosseir 1981; Dauptain *et al.* 2010) have shown that the instabilities in the shear layer are intensified when the nozzle-to-wall distance, h, is shorter than the inviscid core of the jet. Considering this observation, in order to study the effect of nozzle-to-wall distance on the receptivity at the nozzle lip, two nozzle-to-wall distances of $2d$ and $5d$ are investigated, which based on Ho & Nosseir (1981) and our numerical experiment lie within the potential core which for a jet with an $NPR = 3.4$ is larger than $7.5d$. The significance of the impinging plate located at $2d$ is that a dominant impingement tone was observed, while the significance of the impinging plate located at $5d$ is its potential to allow the spatial development of large structures and their interactions with the shocks.

The size of the domain in the radial direction is $12d$ (figure 5). The details of the computational grid for the two cases are provided in table 2. A uniform grid is employed in the azimuthal direction, θ. In the axial direction, x, a fine grid is used near the nozzle and near the impingement wall. In the radial direction, r, a fine grid is used in the mixing layer region with a polynomial stretching of the grid points towards the centre of the jet and the far-field. The locations of the radial and axial grid points are shown in the figure 6 for the sake of completeness. Note that the maximum mesh spacing of 0.04 for $r < 8.5$ allows the capture of the propagation of acoustic waves with Strouhal number up to 5.0 in the LESs. The mean inlet axial velocity is specified using the hyperbolic-tangent function of Bodony & Lele (2005) with the non-dimensionalised inlet momentum thickness of 0.04 which is comparable to that of previous studies (Bogey *et al.* 2011). The inlet velocity is free of any synthetic turbulence in order to permit future comparison with experimental data as the experimental nozzles of the under-expanded supersonic impinging jet typically have a very high contraction ratio, which results in a very low turbulence level of the issuing jet (Edgington-Mitchell *et al.* 2014*a*). The Reynolds number is 50,000 which is approximately an order-of-magnitude lower than used in experimental studies. This Reynolds number is chosen to maintain the LES resolution requirement at acceptable computational cost (Kawai & Lele 2010).

Figure 7 shows the contour maps of the instantaneous density-gradient field for the two

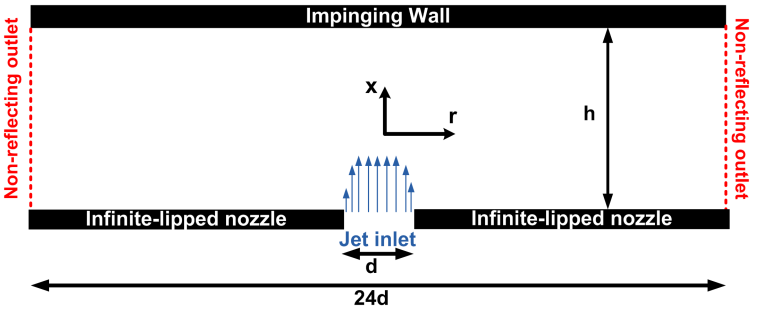

FIGURE 5. Schematic of the domain and the configuration of this study.

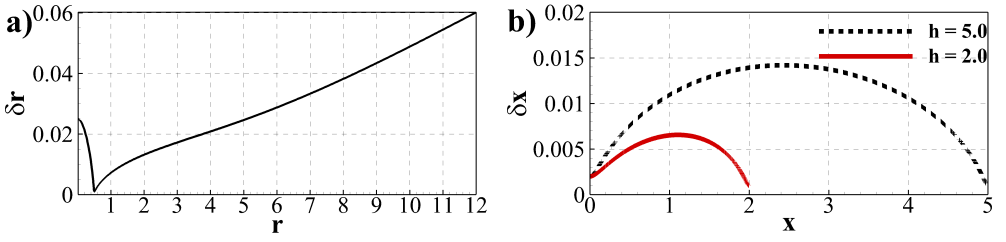

FIGURE 6. a) radial and b) axial mesh spacing.

cases of this study with nozzle-to-wall distances (a) $h = 2d$ and (b) $h = 5d$, respectively. The development of instabilities in the shear layer as well as the travelling acoustic waves (*i.e.* the dashed red curves), which are two of the main components of the feedback loop in under-expanded supersonic impinging jets are clearly observable. Furthermore, in Figure 7 (b), the $h = 5d$ case, clearly shows a reflected acoustic wave from the infinite lip. Before reading further, the interested reader may consult animations of the density gradients presented in figure 7 which is presented in the on-line supplementary animations to this paper available at Please place the link to the both supplementary movies here. This animation is quite instructive to gain an overall picture of flow and acoustic paths.

4. Results and discussion

4.1. *Mean flow fields*

The linearised Navier-Stokes equations require a mean flow, which in this study is the mean flow field. The ensemble average of any non-dimensionalised variable ϕ is computed as the temporal and azimuthal mean given by the following equation,

$$\bar{\phi}(x,r) = \frac{1}{N_t \times N_\theta} \sum_{i=1}^{N_t} \sum_{j=1}^{N_\theta} \phi(x,r,\theta_j,t_i), \tag{4.1}$$

where N_t is the number of snapshots over which the average is computed and N_θ is the number of azimuthal grids. The mean flow field for each case is obtained using the equation 4.1 over 200 acoustic time units of the statistically stationary LES.

Figure 8 shows the contour plots of the ensemble-averaged axial and radial velocities, as well as ensemble-averaged pressure fields for $h = 2d$ (a-c) and $h = 5d$ (d-f). Figure 8 (a) and (d) show the mean streamwise velocities. The streamlines are shown in the zoomed sub-frame, near the nozzle exit and the impingement wall. The initial expansion

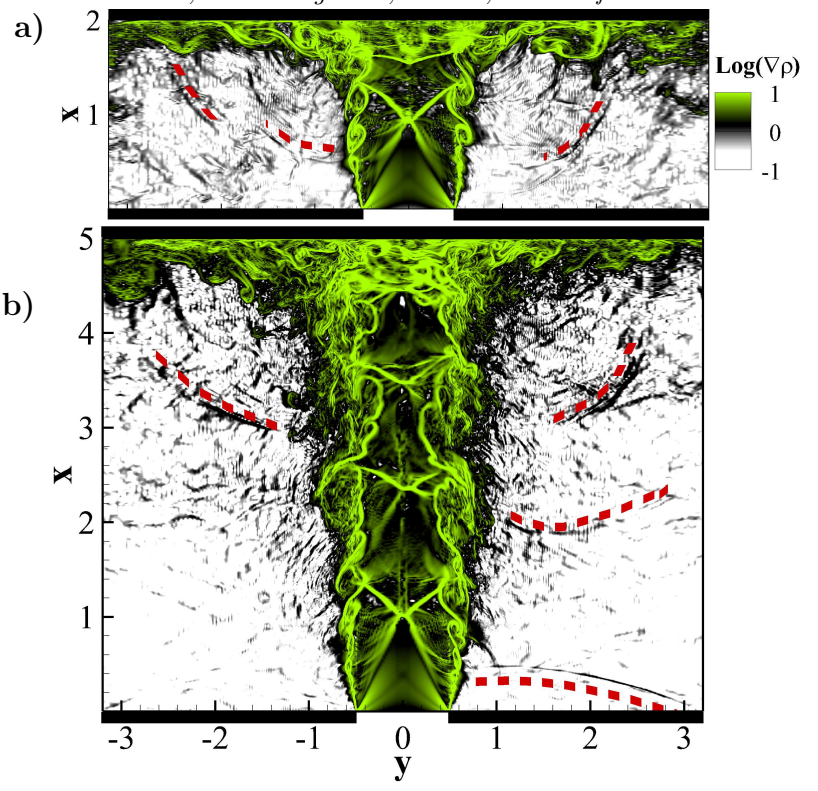

FIGURE 7. Instantaneous contour plots of the density gradient for h a) 2 and b) 5 (y is related to radius by $-r < y < r$)

.

of the shear layer upon exit from the nozzle is visible for both nozzle-to-wall distances. There is a high level of entrainment near the nozzle in the region marked by 'A' and 'D' (figure 8 (a) and (d)). This is clearer in the zoomed sub-frame where the streamlines are visualised. The velocity vectors are directed perpendicularly towards the jet except very close to the nozzle where they move towards the nozzle and then close to the nozzle turn parallel to the jet edge into the jet direction. A small Mach disk with a size of less than 0.05 jet diameters is also noticed at $x \approx 1.0$, marked with a 'B' and 'E' in figures 8 (a) and (d), respectively. The small size of the Mach disk is due to the low NPR of 3.4 (Edgington-Mitchell *et al.* 2014*b*). Other classical features of an under-expanded supersonic jet such as a triple point and an oblique shock are also visible.

An evident expansion and contraction of the jet boundary are also observed, which is a characteristic of under-expanded supersonic jets (Raman 1997). An interesting parameter is the cell length (*i.e.* the wavelength of the wave-shape periphery of the jet as shown by dashed-dot blue curves in figures 8 (a) and (d). Prandtl (1904) proposed his well-known formula to approximate the cell length based on the small perturbation theory. This formula has a form of $\lambda/d = A\sqrt{(NPR - NPR_c)}$ where λ is the cell length, A is the model constant and NPR_c is the critical nozzle-pressure-ratio. He found a value of 1.22 for the model constant A. Based on extensive measurement of cell lengths in photographs of choked jets, Emden (1899) proposed a value of 0.88 for A. These two constants result in two cell lengths of 1.47 and 1.08. The LES results show cell lengths of 1.4 and 1.2 for the nozzle-to-wall distance of $2d$ and $5d$, respectively.

Upon impingement, a recirculation bubble is observed and labelled 'C' in figure 8

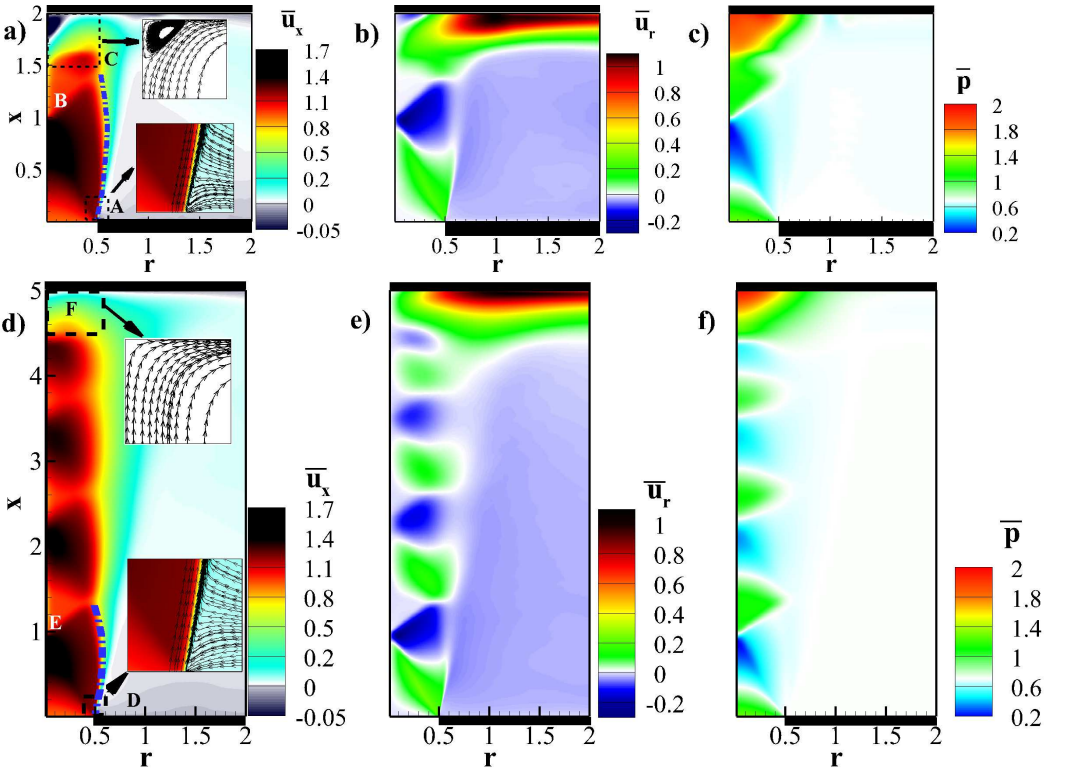

FIGURE 8. Ensemble averaged a, d) streamwise velocity, b, e) radial velocity and c, f) pressure for nozzle–to–wall distances of $2d$ (a-c) and $5d$ (d-f).

(a) for the case with the nozzle-to-wall distance of $2d$ while there is no evidence of the recirculation zone for the nozzle-to-wall-distance of $5d$ labelled as 'E' in figure 8 (d). This is easy to retrieve from the streamlines of the flow field in this region, as presented in the zoomed subframe. The contour maps of the radial velocity are presented in figures 8 (b) and (e). The triple point and oblique shock are easily perceived in these plots. The negative mean radial velocity in the region outside of the jet confirms the presence of entrainment. The formation of a strong wall jet at the impingement wall is clearly observable. Negative radial velocity at the impingement is noticed for the nozzle-to-wall distance of $2d$, which once again confirms the recirculation bubble, while there is no negative radial velocity in the case of $h = 5d$. The ensemble-averaged pressure fields are presented in figures 8 (c) and (f). There is a pressure drop before the Mach disk. There is also a high-pressure region at the impingement region as the flow is stagnated and a stand-off shock is formed. This region is slightly wider in streamwise direction for the nozzle-to-wall distance of $2d$. The modulation of the pressure fields can be seen in both cases, but clearly it is stronger for the shorter nozzle-to-wall distance of $2d$.

4.2. *Receptivity analysis*

Using the mean flow fields obtained from ensemble averaging of the LES results, the linearised Navier-Stokes equations are solved with the same LES resolution in a smaller domain in the radial direction, *i.e.* $4.9d$ in the radial direction with a maximum mesh spacing of 0.022 in the radial direction for this domain. The propagation of acoustic waves with Strouhal number up to 9 can be captured accurately with the linearised simulations. A sixth-order central finite difference method and fourth-order five-step Runge-Kutta are

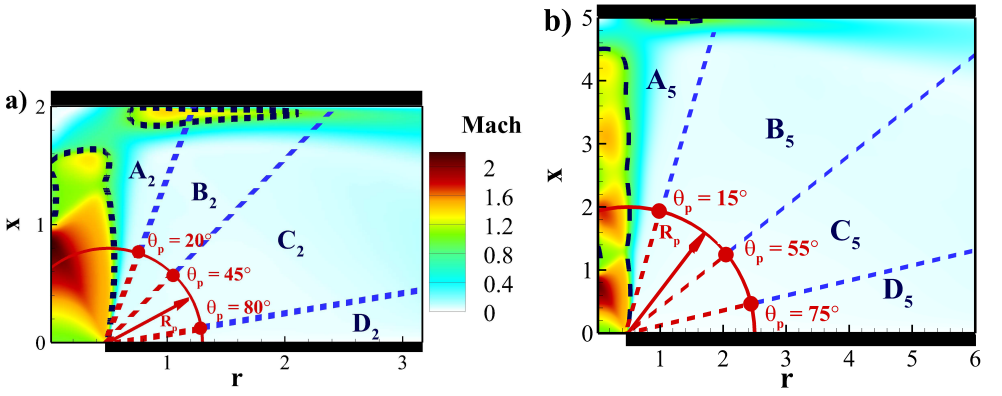

FIGURE 9. Colormaps of local Mach number for the nozzle-to-wall distance of a) $2d$ and $5d$ (Dashed black iso-lines are local Mach number of unity, solid red circle shows the location of the impulse in the impulse simulations with critical angles from the centreline for each case is marked).

used for the spatial discretisation and temporal integration, respectively (Stegeman *et al.* 2016*a*; Karami *et al.* 2018*b*). The linearised analysis is performed using the parameters presented in table 1.

In order to facilitate the discussion, the contour maps of the ensemble-averaged local Mach number defined as the ensemble-averaged local velocity normalised by the ensemble-averaged local speed of sound ($\sqrt{\gamma P/\rho}$) are presented in figure 9. In this figure, the dashed black line shows the sonic line. The regions A to D are marked based on the significant variations in the transfer function as the angular location of the acoustic impulse is varied to facilitate the discussion.

The transfer function quantifying the receptivity is obtained using the method described in section 2. The impulse excites a wide range of frequencies, thus providing the spectrum of the transfer function. The transfer function, G, for the nozzle-to-wall distance of $2d$ and $5d$ are presented in figures 10 and 11 for azimuthal mode-numbers of (a) $m = 0$, (b) $m = 1$ and (c) $m = 2$. The red and black dashed lines indicate 90 and 95 percent of the maximum value of the transfer function, respectively. The contour level is logarithmic to ensure that the changes in G are visible. This analysis shows that the impulses in the vicinity of the impingement wall have the highest amplification in both nozzle-to-wall distance cases. The main findings are summarised as follows,

- **Nozzle-to-wall distance of $2d$ (figures 9 (a) and 10)**:
  - The transfer function has its minimum value for the acoustic impulse located at an angular position less than 20° (region labelled as A_2 in figure 9 (a)). This is due to the blockage of the acoustic waves by the expanded shear layer of the jet. This is clear as the sonic line bulges out at $x \approx 0.5$, resulting in acoustic waves being blocked form directly reaching the nozzle lip. This is consistent with the experimental observation of Raman (1997).
  - A pressure impulse in the region B_2 ($20° < \theta_p < 45°$) travels towards the nozzle and reaches the nozzle lip directly. The transfer function shows amplification of an input signal over a broad range of frequencies with a maximum transfer function at a Strouhal number of 4.0 which is insensitive to the angular position of the impulse for the axisymmetric azimuthal mode. In contrast, for higher azimuthal mode-numbers,

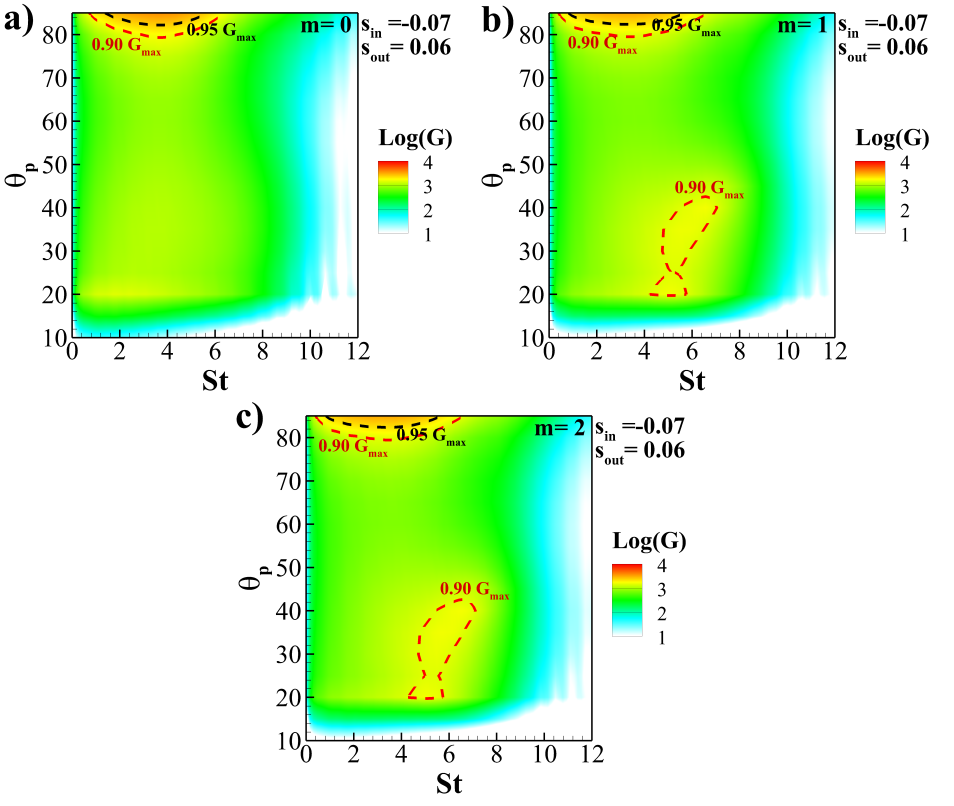

FIGURE 10. Contour of the logarithm of the transfer function, G, for the nozzle-to-wall distance of $2d$ for azimuthal mode-numbers (a) $m = 0$, (b) $m = 1$ and (c) $m = 2$ (The 90 and 95 percent of the maximum value of the transfer function is marked with red and black dashed lines, respectively.).

the maximum transfer function shifts towards a higher Strouhal number as the angular position of the acoustic impulse increases.

- A low amplification of the input signal occurs if the impulse is located between angles of 45° and 80° (marked as C_2). This is consistent among all the azimuthal mode-numbers.
- The maximum amplification of an input signal occurs if the pressure impulse is located near the nozzle lip, *i.e.* the angle from the jet axis is more than 80°. This region is labelled by D_2. The input signal is amplified over a wide range of frequencies with Strouhal numbers in the range of 0.5 to 6.2. The peak of the amplification occurs at the Strouhal number of 3.0. This broad-spectrum is due to the nozzle lip (Raman 1997; Rogler & Reshotko 1975). The optimal amplification of the impulse in the vicinity of the nozzle lip is independent of the azimuthal mode-number. A similar behaviour is observed for all three azimuthal mode-numbers of 0, 1 and 2.

- **Nozzle-to-wall distance of $5d$ (figures 9 (b) and 11)**:
  - An input signal generated by a pressure impulse located in the region A_5 (*i.e.* for angles between 10° and 15°) is slightly amplified by the nozzle lip and the transfer function has a small value. This is similar to the smaller nozzle-to-wall distance, and the same hypothesis applies – the expanded shear layer blocks the acoustic waves

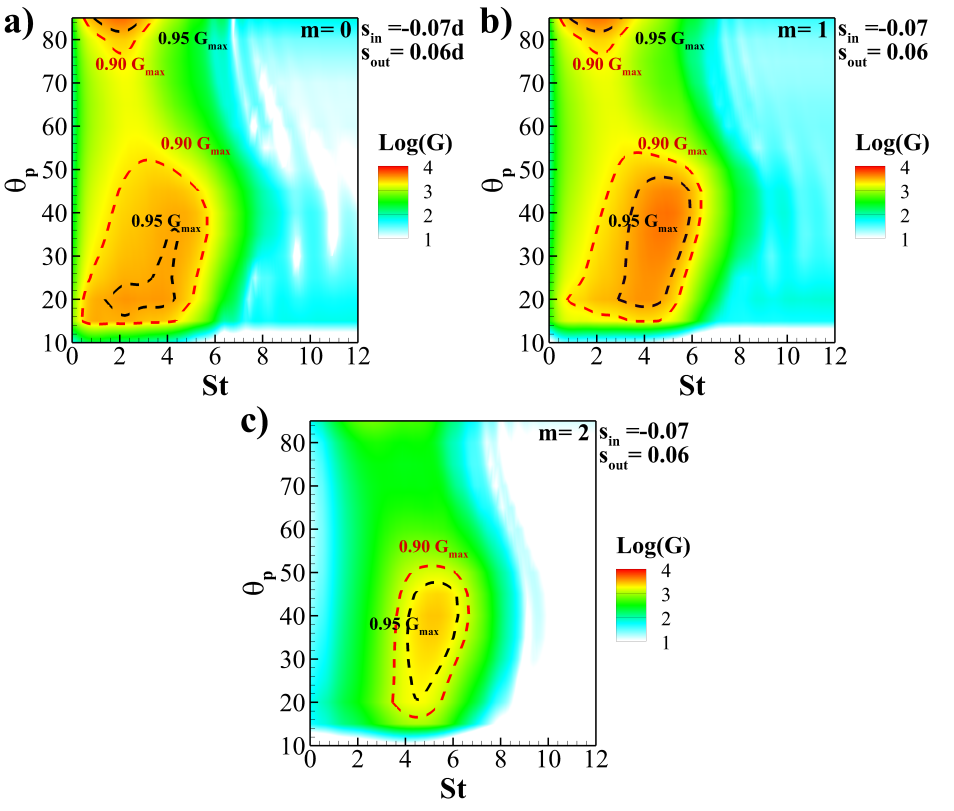

FIGURE 11. Contour of the logarithm of the transfer function, G, for the nozzle-to-wall distance of $5d$ for azimuthal mode-numbers (a) $m = 0$, (b) $m = 1$ and (c) $m = 2$ (The 90 and 95 percent of the maximum value of the transfer function is marked with red and black dashed lines, respectively.).

from direct view. However, as the nozzle-to-wall distance is higher compared to the previous case, the angular limit is slightly narrower.

- For the pressure impulse located in the region B_5 ($15° < \theta_p < 55°$), the transfer function shows the maximum amplification of the input signal. All three azimuthal mode-numbers show a high amplification of an incoming signal with the azimuthal mode-number of 2 (*i.e.* helical mode) being dominant. A high amplification occurs over a wide range of frequencies (*i.e.* a broad range of Strouhal numbers) for the first two azimuthal mode-numbers, while occurring over a narrower frequency band for the azimuthal mode-number of 2. The maximum value of the transfer function depends on the angular position of the impulse in this region. As the location of the pressure impulse moves towards the infinite-lipped nozzle wall, the Strouhal number of the maximum transfer function increases for all three azimuthal mode-numbers.
- The receptivity of the nozzle lip to acoustic waves created by a pressure impulse located in the region C_5 is limited to the low-frequency band. The peak of the transfer function is shifted to the low-frequency band as the impulse location moves towards the infinite-lipped nozzle wall for the azimuthal mode-numbers of 0 and 1, while it is independent of the impulse location for the azimuthal mode-number of 2. The amplification of an incoming signal occurs in a slightly narrower frequency

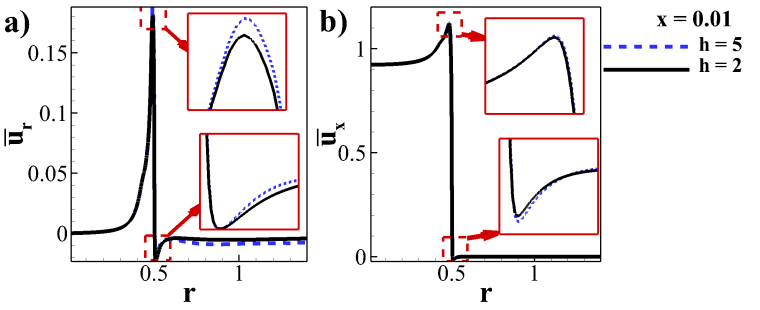

FIGURE 12. The profiles of the ensemble-averaged a) radial and b) streamwise velocities at $x = 0.01$ for both nozzle-to-wall distances of 2 jet diameters (solid black line) and 5 jet diameters (dashed blue line).

range compared to the incoming signal generated by an impulse located in the region B_5.

- The second maximum of the transfer function occurs when the pressure impulse is located near to the infinite-lipped nozzle in the region D_5 and only exists for the axisymmetric and helical modes, *i.e.* $m = 0$ and 1. In contrast to $h = 2d$, high amplification is observed in narrowband low frequencies, *i.e.* low Strouhal numbers.

The observed differences in the receptivity for the $h = 2d$ and $h = 5d$ cases provided quantitatively via the computed transfer functions are a consequence of the base ingredient to the linearised Navier-Stokes solutions, namely the mean flow field (Beneddine *et al.* 2016).

Figures 12 (a) and (b) show the profiles of the ensemble-averaged radial and streamwise velocities at $x = 0.01$, respectively. There are clear differences in the ensemble-averaged radial velocity, indicating slightly higher entrainment in the case of $h = 2d$. The ensemble-averaged streamwise velocity has a negative value outside of the jet's periphery where this negative value is slightly higher for the case of $h = 5d$.

5. Conclusion

The receptivity at the nozzle lip of under-expanded supersonic impinging jets has been investigated. A transfer function is defined to quantify the receptivity as the ratio of the total energy of the input irrotational acoustic signal to the output vortical fluid dynamic signal at the nozzle lip. The linearised three-dimensional Navier-Stokes equations are solved using an acoustic impulse to simulate a sound source. The acoustic pulse is located at the fixed radius and variable angle from the jet axis. This allows the investigation of the sensitivity of the transfer function to the acoustic impulse location and the azimuthal mode-number. It has been demonstrated that the nozzle lip has the highest transfer function when the acoustic field originates from an acoustic source located close to the wall which forms the infinite-lipped nozzle. This is consistent for the first two azimuthal mode-numbers for both nozzle-to-wall distances except for acoustic disturbances which have an azimuthal mode-number of 2 when $h = 5d$. In this case, the results indicate that there is a second maximum in the transfer function, which occurs when the acoustic field originates from an acoustic impulse located in the region halfway between the infinite-lipped nozzle surface and the shear layer, *i.e.* for angles between 15° and 50°.

The most striking conclusion to emerge from this analysis is the suggestions for effective control of instabilities in under-expanded supersonic impinging jets and hence, the

elimination or minimisation of self-sustained oscillations in under-expanded supersonic impinging jets. The two nozzle-to-wall distances of $2d$ and $5d$ of this study have demonstrated the sensitivity of the receptivity to the angular location of acoustic sources. For under-expanded supersonic impinging jets with a nozzle-to-wall distance of $2d$, the receptivity at the nozzle lip is dominated primarily by acoustic sources that are located at angular positions greater than 80° from the jet centreline. Whereas for $h = 5d$, there are two angular locations where the acoustic waves originating from an acoustic impulse significantly influence the receptivity at the nozzle lip. One is at angular locations greater than 80° from the jet centreline, which is similar to the nozzle-to-wall distances of $2d$ case, while the other is an angular region bounded between 15° to 55° from the jet centreline. This behaviour indicates the dynamic nature of the instabilities, highlighting the practical difficulties that arise in using a passive control strategies for effective control in the industrial applications where the nozzle-to-wall distance changes rapidly. However, when the nozzle-to-wall distance is fixed, a passive control strategy to control the instabilities would be the elimination of acoustic waves which are reflected by near surfaces including the infinite-lipped nozzle surface. This can be achieved by a properly designed sound absorber attached to the reflective surfaces.

Acknowledgements

This work was supported by the Australian Research Council. The research benefited from computational resources provided through the National Computational Merit Allocation Scheme, supported by the Australian Government. The computational facilities supporting this project included the Australian NCI Facility, the partner share of the NCI facility provided by Monash University through a ARC LIEF grant, Pawsey Supercomputing Centre and the Multi-modal Australian ScienceS Imaging and Visualisation Environment (MASSIVE).

REFERENCES

Ackeret, J. 1927 Gasdynamik pp. 289–342.

Amili, O., Edgington-Mitchell, D., Honnery, D. & Soria, J. 2016 Interaction of a supersonic underexpanded jet with a flat plate. In *Fluid-Structure-Sound Interactions and Control*, pp. 247–251. Springer.

Barkley, D. 2006 Linear analysis of the cylinder wake mean flow. *EPL (Europhysics Letters)* **75** (5), 750.

Barone, M. F. & Lele, S. K. 2005 Receptivity of the compressible mixing layer. *J. Fluid Mech.* **540**, 301–335.

Bechert, D. W. 1988 Excitation of instability waves in free shear layers Part 1. theory. *J. Fluid Mech.* **186**, 47–62.

Bechert, D. W. & Stahl, B. 1988 Excitation of instability waves in free shear layers Part 2. experiments. *J. Fluid Mech.* **186**, 63–84.

Bendat, J. S. & Piersol, A. G. 2011 *Random data: analysis and measurement procedures*, , vol. 729. John Wiley & Sons.

Beneddine, S., Sipp, D., Arnault, A., Dandois, J. & Lesshafft, L. 2016 Conditions for validity of mean flow stability analysis. *J. Fluid Mech.* **798**, 485–504.

Bodony, D. J. & Lele, S. K. 2005 On using large-eddy simulation for the prediction of noise from cold and heated turbulent jets. *Phys. Fluids* **17** (8), 085103.

Bogey, C., Marsden, O. & Bailly, C. 2011 Large-eddy simulation of the flow and acoustic fields of a reynolds number 10^5 subsonic jet with tripped exit boundary layers. *Phys. Fluids* **23** (3), 035104.

Dauptain, A., Cuenot, B. & Gicquel, L. Y. M. 2010 Large eddy simulation of stable supersonic jet impinging on flat plate. *AIAA journal* **48** (10), 2325–2338.

Donaldson, C., Snedeker, R. S. *et al.* 1971 A study of free jet impingement. Part 1. Mean properties of free and impinging jets. *J. Fluid Mech.* **45** (2), 281–319.

Edgington-Mitchell, D., Honnery, D. R. & Soria, J. 2014*a* The underexpanded jet mach disk and its associated shear layer. *Phys. Fluids* **26** (9), 1578.

Edgington-Mitchell, D., Oberleithner, K., Honnery, D. R. & Soria, J. 2014*b* Coherent structure and sound production in the helical mode of a screeching axisymmetric jet. *J. Fluid Mech.* **748**, 822–847.

Emden, R. 1899 Ueber die ausstromungserscheinungen permanenter gase. *Annalen der Physik* **305** (9), 264–289.

Erturk, E. & Corke, T. C. 2001 Boundary layer leading-edge receptivity to sound at incidence angles. *J. Fluid Mech.* **444**, 383–407.

Gojon, R. & Bogey, C. 2017 Flow structure oscillations and tone production in underexpanded impinging round jets. *AIAA Journal* .

Gojon, R., Bogey, C. & Marsden, O. 2015 Large-eddy simulation of underexpanded round jets impinging on a flat plate 4 to 9 radii downstream from the nozzle. *AIAA Paper* **2210**, 2015.

Haddad, O. M. & Corke, T. C. 1998 Boundary layer receptivity to free-stream sound on parabolic bodies. *J. Fluid Mech.* **368**, 1–26.

Hammond, D. A. & Redekopp, L. G. 1997 Global dynamics of symmetric and asymmetric wakes. *J. Fluid Mech.* **331**, 231–260.

Henderson, B., Bridges, J. & Wernet, M. 2005 An experimental study of the oscillatory flow structure of tone-producing supersonic impinging jets. *J. Fluid Mech.* **542**, 115–137.

Henderson, B. & Powell, A. 1993 Experiments concerning tones produced by an axisymmetric choked jet impinging on flat plates. *J. Sound Vib.* **168** (2), 307–326.

Henderson, L. F. 1966 Experiments on the impingement of a supersonic jet on a flat plate. *Zeitschrift für angewandte Mathematik und Physik ZAMP* **17** (5), 553–569.

Ho, C-M. & Nosseir, N. S. 1981 Dynamics of an impinging jet. Part 1. The feedback phenomenon. *J. Fluid Mech.* **105**, 119–142.

Illingworth, S. J., Monty, J. P. & Marusic, I. 2018 Estimating large-scale structures in wall turbulence using linear models. *J. Fluid Mech.* **842**, 146–162.

Jones, D. S. & Morgan, J. D. 1973 The instability due to acoustic radiation striking a vortex sheet on a supersonic stream. *Proceedings of the Royal Society of Edinburgh Section A: Mathematics* **71** (2), 121–140.

Jones, D. S. & Morgan, J. P. 1972 The instability of a vortex sheet on a subsonic stream under acoustic radiation. In *Mathematical Proceedings of the Cambridge Philosophical Society*, , vol. 72, pp. 465–488. Cambridge University Press.

Karami, S., Edgington-Mitchell, D. & Soria, J. 2018*a* Large eddy simulation of supersonic under-expanded jets impinging on a flat plate. In *Proceedings of the 11th Australasian Heat and Mass Transfer Conference*, p. 12.

Karami, S. & Soria, J. 2018 Analysis of coherent structures in an under-expanded supersonic impinging jet using spectral proper orthogonal decomposition (SPOD). *Aerospace* **5** (3), 73.

Karami, S., Stegeman, P. C., Ooi, A. & Soria, J. 2019 High-order accurate large-eddy simulations of compressible viscous flow in cylindrical coordinates. *Computers & Fluids* p. 104241.

Karami, S., Stegeman, P. C., Theofilis, V., Schmid, P. J. & Soria, J. 2018*b* Linearised dynamics and non-modal instability analysis of an impinging under-expanded supersonic jet. In *Journal of Physics: Conference Series*, , vol. 1001, p. 012019. IOP Publishing.

Kawai, S. & Lele, S. K. 2010 Large-eddy simulation of jet mixing in supersonic crossflows. *AIAA journal* **48** (9), 2063–2083.

Kennedy, C. A. & Carpenter, M. H. 1994 Several new numerical methods for compressible shear-layer simulations. *Appl. Numer. Math.* **14** (4), 397 – 433.

Kennedy, C. A., Carpenter, M. H. & Lewis, R. M. 2000 Low-storage, explicit Runge–Kutta schemes for the compressible Navier–Stokes equations. *Appl. Numer. Math.* **35** (3), 177 – 219.

Kerschen, E. 1996 Receptivity of shear layers to acoustic disturbances. In *Theroretical Fluid Mechanics Conference*, p. 2135.

Li, S., Muddle, B., Jahedi, M. & Soria, J. 2012 A numerical investigation of the cold spray process using underexpanded and overexpanded jets. *J. Therm. Spray Technol.* **21**, 108 – 120.

Lilly, D. K. 1992 A proposed modification of the Germano subgrid-scale closure method. *Phys. Fluids A: Fluid Dynamics* **4** (3), 633–635.

Mason-Smith, N., Edgington-Mitchell, D., Buchmann, N. A., Honnery, D. R. & Soria, J. 2015 Shock structures and instabilities formed in an underexpanded jet impinging on to cylindrical sections. *Shock Waves* **25** (6), 611–622.

Mittal, S. 2008 Global linear stability analysis of time-averaged flows. *Int. J. Numer. Methods Fluids* **58** (1), 111–118.

Morgan, J. D. 1974 The interaction of sound with a semi-infinite vortex sheet. *The Quarterly Journal of Mechanics and Applied Mathematics* **27** (4), 465–487.

Morkovin, M. V. 1969 Critical evaluation of transition from laminar to turbulent shear layers with emphasis on hypersonically traveling bodies. *Tech. Rep.*. AFFDL TR, 68–149.

Oberleithner, K., Rukes, L. & Soria, J. 2014 Mean flow stability analysis of oscillating jet experiments. *J. Fluid Mech.* **757**, 1–32.

Pier, B. 2002 On the frequency selection of finite-amplitude vortex shedding in the cylinder wake. *J. Fluid Mech.* **458**, 407–417.

Poinsot, T. & Lele, S. K. 1992 Boundary conditions for direct simulations of compressible viscous flows. *J. Comput. Phys.* **101** (1), 104 – 129.

Powell, A. 1988 The sound-producing oscillations of round underexpanded jets impinging on normal plates. *The Journal of the Acoustical Society of America* **83** (2), 515–533.

Prandtl, L. 1904 Über die stationären Wellen in einem Gasstrahl. *Physikalische Zeitschrift* **5**, 599–6010.

Prandtl, L. 1907 Neue Untersuchungen über die strömende Bewegung der Gase und Dämpfe. *Physikalische Zeitschrift* **8**, 23–30.

Prandtl, L. 1913 Gasbewegung. *Handwörterbuch der Naturwissenschaften* **4**, 544–560.

Raman, G. 1997 Cessation of screech in underexpanded jets. *J. Fluid Mech.* **336**, 69–90.

Raman, G. & Srinivasan, K. 2009 The powered resonance tube: from hartmann's discovery to current active flow control applications. *Prog. Aerosp. Sci.* **45** (4-5), 97–123.

Reshotko, E. 1976 Boundary-layer stability and transition. *Annu. Rev. Fluid Mech.* **8** (1), 311–349.

Reshotko, E. 1984 Environment and receptivity. In *AGARD Spec. Course on Stability and Transition of Laminar Flow 11 p (SEE N84-33757 23-34)*.

Risborg, A. & Soria, J. 2009 High-speed optical measurements of an underexpanded supersonic jet impinging on an inclined plate. In *28th International Congress on High-Speed Imaging and Photonics* (ed. Harald Kleine & Martha Patricia Butron Guillen), , vol. 7126, pp. 477 – 487. International Society for Optics and Photonics, SPIE.

Rogler, H. L. & Reshotko, E. 1975 Disturbances in a boundary layer introduced by a low intensity array of vortices. *SIAM Journal on Applied Mathematics* **28** (2), 431–462.

Rossiter, J. E. 1964 Wind tunnel experiments on the flow over rectangular cavities at subsonic and transonic speeds. *Tech. Rep.*. Ministry of Aviation; Royal Aircraft Establishment; RAE Farnborough.

Rowley, C. W. 2002 Modeling, simulation, and control of cavity flow oscillations. PhD thesis, California Institute of Technology.

Rowley, C. W., Colonius, T. & Basu, A. J. 2002 On self-sustained oscillations in two-dimensional compressible flow over rectangular cavities. *J. Fluid Mech.* **455**, 315–346.

Ruban, A. I., Bernots, T. & Kravtsova, M. A. 2016 Linear and nonlinear receptivity of the boundary layer in transonic flows. *J. Fluid Mech.* **786**, 154–189.

Sartor, F., Mettot, C., Bur, R. & Sipp, D. 2015 Unsteadiness in transonic shock-wave/boundary-layer interactions: experimental investigation and global stability analysis. *J. Fluid Mech.* **781**, 550–577.

Sasaki, K., Vinuesa, R., Cavalieri, A. V. G., Schlatter, P. & Henningson, D. S. 2019 Transfer functions for flow predictions in wall-bounded turbulence. *J. Fluid Mech.* **864**, 708–745.

Sipp, D. & Lebedev, A. 2007 Global stability of base and mean flows: a general approach and its applications to cylinder and open cavity flows. *J. Fluid Mech.* **593**, 333–358.

Soria, J. & Risborg, A. 2019 High-speed optical measurements of an under-expanded supersonic jet impinging on an inclined plate. `https://monash.figshare.com/articles/High-speed_optical_measurements_of_an_under-expanded_supersonic_jet_impinging_on_an_inclined_plate_/10006427`.

Stegeman, P. C., Ooi, A. & Soria, J. 2015 Proper orthogonal decomposition and dynamic mode decomposition of under-expanded free-jets with varying nozzle pressure ratios. In *Instability and Control of Massively Separated Flows*, pp. 85–90. Springer.

Stegeman, P. C., Pérez, J. M., Soria, J. & Theofilis, V. 2016*a* Inception and evolution of coherent structures in under-expanded supersonic jets. In *Journal of Physics: Conference Series*, , vol. 708, p. 012015.

Stegeman, P. C., Soria, J. & Ooi, A. 2016*b* Interaction of shear layer coherent structures and the stand-off shock of an under-expanded circular impinging jet. In *Fluid-Structure-Sound Interactions and Control*, pp. 241–245.

Tam, C. K. W. 1986 Excitation of instability waves by sound —A physical interpretation. *J. Sound Vib.* **105** (1), 169 – 172.

Tam, C. K. W. & Ahuja, K. K. 1990 Theoretical model of discrete tone generation by impinging jets. *J. Fluid Mech.* **214**, 67–87.

Turton, S. E., Tuckerman, L. S. & Barkley, D. 2015 Prediction of frequencies in thermosolutal convection from mean flows. *Physical Review E* **91** (4), 043009.

Wanderley, J. B. V. & Corke, T. C. 2001 Boundary layer receptivity to free-stream sound on elliptic leading edges of flat plates. *J. Fluid Mech.* **429**, 1–21.

Weightman, J. L., Amili, O., Honnery, D., Edgington-Mitchell, D. & Soria, J. 2017 On the effects of nozzle lip thickness on the azimuthal mode selection of a supersonic impinging flow. In *23rd AIAA/CEAS Aeroacoustics Conference*, p. 3031.